Vibrational Properties of Monophosphate Tungsten Bronzes $(PO_2)_4(WO_3)_{2m}$ ($m = 4, 6$)

Z.-T. Zhu

Department of Chemistry, State University of New York at Binghamton, Binghamton, New York 13902

J. L. Musfeldt*

Department of Chemistry, University of Tennessee, Knoxville, Tennessee 37996

Z. S. Teweldemedhin and M. Greenblatt

Department of Chemistry, Rutgers, The State University of New Jersey, Piscataway, New Jersey 08855

Received March 9, 2001. Revised Manuscript Received June 25, 2001

We report the vibrational properties of quasi-two-dimensional charge density wave (CDW) materials $(PO_2)_4(WO_3)_{2m}$ ($m = 4, 6$). The CDW transitions occur at 80 and 54 K for $m = 4$ and 120 and 60 K for $m = 6$. The polarized middle infrared response clearly demonstrates the two-dimensional character of both compounds, with strong vibrational modes and low reflectance along the interlayer direction (*c*) but screened vibrational modes and high reflectance in the conducting (*ab*) plane. The temperature dependence of the vibrational modes is weak for the $m = 4$ compound, whereas the spectrum of the $m = 6$ material displays mode splitting and additional fine structure in the CDW states. The results are discussed in terms of the CDW formation and structural changes at low temperature.

I. Introduction

Charge density waves (CDW) in quasi-two-dimensional (Q2D) materials such as some layered dichalcogenides, molybdenum bronzes, and phosphate tungsten bronzes have attracted considerable attention.[1−3] In these Q2D systems, electron−phonon coupling drives the gap opening and concomitant nesting of the Fermi surface, but an imperfect nesting vector often leads to small residual Fermi pockets in the CDW state; therefore, a metal → metal transition is observed in the Q2D CDW systems.[4] While the science of one-dimensional (1D) CDWs underlies and is certainly relevant to Q2D solids, the Q2D oxides are unique in their own right.[5] The vibrational properties of well-nested quasi-one-dimensional density wave compounds have been investigated in the past;[6−15] less is known about the imperfectly nested materials.

Monophosphate tungsten bronzes (MPTBs) are a series of compounds with general chemical formula $(PO_2)_4(WO_3)_{2m}$ ($m = 2-14$).[3] The structure of these materials is based on ReO_3-type slabs of corner-sharing WO_6 octahedral connected by PO_4 tetrahedra. The conduction electrons are located at the center of the octahedra blocks, leading to the Q2D electronic properties and Fermi surface.[16−19] Since the number of conduction electrons in the primitive unit cell is always 2, the concentration of free carriers decreases as $2/m$ with increasing *m*. Meanwhile, the dimensionality decreases with increasing *m*, because increased thickness of octahedra slabs (along the *c*-axis) weakens interactions between conduction layers. Thus, $(PO_2)_4(WO_3)_{2m}$ ($m = 2-14$) provides a very good model system with which to study free carrier concentration, imperfect Fermi surface nesting, and dimensionality effects in Q2D CDWs.

(1) *Low Dimensional Electronic Properties of Molybdenum Bronzes and Oxides*; Schlenker, C., Ed.; Kluwer: Dordrecht, 1989.
(2) *Oxide Bronzes*; Greenblatt, M., Ed.; World Scientific: Singapore, 1993 (*Int. J. Mod. Phys. B* **1993**, *7* (23 & 24).
(3) Greenblatt, M. *Acc. Chem. Res.* **1996**, *29*, 219.
(4) Canadell, E.; Whangbo, M.-H. *Chem. Rev.* **1991**, *91*, 965.
(5) Sandre, E.; Foury-Leylekian, P.; Ravy, S.; Pouget, J. P. *Phys. Rev. Lett.* **2001**, *86*, 5100.
(6) Karecki, D. R.; Clayman, B. P. *Phys. Rev. B* **1979**, *19*, 6367.
(7) Etemad, S. *Phys. Rev. B* **1981**, *24*, 4959.
(8) Travaglini, G.; Wachter, P. *Phys. Rev. B* **1984**, *30*, 1971.
(9) Degiorgi, L.; Wachter, P.; Greenblatt, M.; McCarroll, W. H.; Ramanujachary, K. V.; Marcus, J.; Schlenker, C. *Phys. Rev. B* **1988**, *38*, 5821.
(10) Jandl, S.; Banville, M.; Pépin, C.; Marcus, J.; Schlenker, C. *Phys. Rev. B* **1989**, *40*, 12487.
(11) Degiorgi, L.; Grüner, G. *Synth. Met.* **1993**, *56*, 2688.
(12) Gorshunov, B. P.; Volkov, A. A.; Kozlov, G. V.; Degiorgi, L.; Blank, A.; Csiba, T.; Dressel, M.; Kim, Y.; Schwartz, A.; Grüner, G. *Phys. Rev. Lett.* **1994**, *73*, 308.
(13) Schwartz, A.; Dressel, M.; Alavi, B.; Blank, A.; Dubois, S.; Grüner, G.; Gorshunov, B. P.; Volkov, A. A.; Kozlov, G. V.; Thieme, S.; Degiorgi, L. *Phys. Rev. B* **1995**, *52*, 5643.
(14) Kanner, G. S.; Gammel, J. T.; Love, S. P.; Johnson, S. R.; Scott, B.; Swanson, B. I. *Phys. Rev. B* **1998**, *50*, 18682.
(15) Bardeau, J.-F.; Bulou, A.; Swanson, B. I.; Hennion, B. *Phys. Rev. B* **1998**, *58*, 2614.
(16) Wang, E.; Greenblatt, M.; Rachidi, I. E.-I.; Canadell, E.; Whangbo, M.-H.; Vadlamannati, S. *Phys. Rev. B* **1989**, *39*, 12969.
(17) Canadell, E.; Whangbo, M.-H.; Rachidi, I. E.-I. *Inorg. Chem.* **1991**, *29*, 3871.
(18) Canadell, E.; Whangbo, M.-H. *Phys. Rev. B* **1991**, *43*, 1894.
(19) Teweldemedhin, Z. S.; Ramanujachary, K. V.; Greenblatt, M. *Phys. Rev. B* **1992**, *46*, 7897.

10.1021/cm010214v CCC: $20.00
Published on Web 08/15/2001

Most of these MPTBs undergo several CDW transitions at low temperature, confirmed by dc resistivity, magnetic susceptibility, and X-ray diffraction measurements.[16,19−26] The $m = 4$ compound shows incommensurate Peierls transitions at $T_{c1} = 80$ K and $T_{c2} = 52$ K [19] with wave vectors $q_1 = (0.330(5),0.292(5),0)$ and $q_2 = (-0.330,0.292,0)$.[27] Two incommensurate CDW transitions in the $m = 6$ material occur at $T_{c1} = 120$ K and $T_{c2} = 60$ K[16] with nesting vectors $q_1 = (0.385,0,0)$ and $q_2 = (0.310,0.295,0)$, respectively.[21] The $m = 7$ compound has a superconducting transition at $T_c = 0.3$ K after two successive CDW transitions at 188 and 60 K.[28] For the compounds with larger values of m, the CDW transitions take place at higher temperature, even above 300 K, likely due to the increased importance of electron−electron interaction and localization effects.[25] The Peierls instabilities of these bronzes are associated with Fermi surface nesting driven by interesting Fermi surface topology.[4] Three sets of diffuse X-ray scattering sheets are observed for both $m = 4$ and 6 compounds,[21] corresponding to the $2k_F$ instabilities of the three "hidden" 1D Fermi sheets along the infinite chains of WO_6 octahedra in the $\vec{a}$ and $\vec{a} \pm \vec{b}$ directions.[5,17,18] These "hidden" 1D surfaces are general features of Q2D oxides and bronzes.[4,5]

Although transport and X-ray studies have revealed that MPTB compounds are Q2D CDW systems, complimentary spectroscopic studies on these prototype materials are rare. There are no reports on the optical properties of these materials and only one photoemission investigation of $(PO_2)_4(WO_3)_{2m}$ ($m = 6$, 10, 12).[29] That spectroscopic studies can provide detailed information on the electronic structure, dimensionality, and lattice dynamics critical to understanding the CDW gap formation and dimensionality effects has been demonstrated by previous studies on molybdenum bronzes and oxides.[9,30,31] The opportunity to investigate the electrodynamics of MPTB $m = 4$ and $m = 6$ compounds in the context of these issues motivates the present work.

II. Symmetry Analysis of $(PO_2)_4(WO_3)_{2m}$

In a study devoted to vibrational properties, a group theory analysis is useful for the assignment and understanding of the infrared and Raman active modes. We can calculate the number of infrared active modes in MPTBs by the correlation method.[32] Both $m = 4$ and $m = 6$ materials have a space group symmetry of $P2_12_12_1$, with site symmetry C_1.[33] Following the very complete analysis procedure for related 2D bronzes, η- and γ-Mo_4O_{11}, presented by McConnell,[34] we have calculated that the mode symmetries of the $m = 4$ and $m = 6$ materials are $\Gamma_{m=4} = 33A + 32B_1 + 32B_2 + 32B_3$ and $\Gamma_{m=6} = 45A + 44B_1 + 44B_2 + 44B_3$. Since the space group $P2_12_12_1$ corresponds to a unit cell symmetry of D_2^4,[32] B_1, B_2, and B_3 modes are infrared active under normal conditions. In sum, $m = 4$ has 96 infrared active modes, and $m = 6$ has 132 infrared active modes.

It is important to realize that the MPTB structures have low site symmetry (C_1), even at 300 K. Therefore, one does not expect, for instance, formal symmetry breaking around the WO_6 octahedra at low temperature. One does, however, anticipate lattice involvement and increased distortion of certain key vibrational modes at the density wave transitions, which may give rise to apparent mode splittings. Our goal is to follow these distortions through the successive CDW transitions in the $m = 4$ and 6 materials.

III. Experimental Section

Single crystals of $P_4W_8O_{32}$ ($m = 4$) and $P_4W_{12}O_{44}$ ($m = 6$) were prepared by standard vapor-transport techniques.[16,19] The structures were confirmed by X-ray diffraction. The crystals are platelike, with the large face defined by the *ab* plane. Typical crystal dimensions are $\sim 2 \times 2 \times 0.3$ mm^3. To prepare the pellets for our transmittance measurements, a tiny portion of a crystal was crushed into powder, mixed with KBr, and compressed under vacuum. The sample was evenly suspended in a KBr matrix, suitable for transmittance measurements.

Polarized middle infrared (600−3000 cm^{-1}) reflectance measurements were performed on single crystals with a Bruker Equinox 55 Fourier transform infrared spectrometer coupled with a Bruker IR Scope II. A 36× objective was used for our reflectance measurements. A nitrogen-cooled MCT detector and standard polarizer set were used to cover the aforementioned energy range. An aluminum mirror was used as a reference for the measurements. Spectral resolution is 2 cm^{-1}. Notice the platelike nature of the crystal with a very small edge along *c* (~0.3 mm) makes the infrared microscopy a necessity. All polarized measurements reported here were carried out on the small edge of the sample.

The middle infrared transmittance spectra of $P_4W_8O_{32}$ and $P_4W_{12}O_{44}$ pellets were measured with a Bruker 113V spectrometer. Low-temperature experiments were carried out with an open-flow cryostat. Spectral resolution is 2 cm^{-1}. The absorption spectrum is calculated from the transmittance as $\alpha(\omega) = -(1/nd) \ln T(\omega)$, where n is the concentration of MPTB in the KBr matrix and d is the pellet thickness.

IV. Results and Discussion

A. Polarization Dependence. Figure 1 displays the reflectance spectra of the $m = 4$ and $m = 6$ MPTB single crystals. In both materials, the spectra are dominated by strong vibrational features when light is polarized along the interlayer direction (*c*-axis). The electronic background is weak, a typical semiconducting response. When the polarization shifts away from the *c*-axis, the

(20) Foury, P.; Pouget, J. P.; Wang, E.; Greenblatt, M. *Europhys. Lett.* **1991**, *16*, 485.
(21) Foury, P.; Pouget, J. P.; Teweldemedhin, Z. S.; Wang, E.; Greenblatt, M. *Synth. Met.* **1993**, *56*, 2605.
(22) Schlenker, C.; Touze, C. L.; Hess, C.; Rötger, A.; Duman, J.; Marcus, J.; Greenblatt, M.; Teweldemedhin, Z. S. *Synth. Met.* **1995**, *70*, 1263.
(23) Ottolenghi, A.; Foury, P.; Pouget, J. P.; Teweldemedhin, Z. S.; Greenblatt, M.; Groult, D.; Marcus, J.; Schlenker, C. *Synth. Met.* **1995**, *70*, 1301.
(24) Foury, P.; Roussel, P.; Groult, D.; Pouget, J. P. *Synth. Met.* **1999**, *103*, 2624.
(25) Dumas, J.; Hess, C.; Schlenker, C.; Bonfait, G.; Marin, E. G.; Groult, D.; Marcus, J. *Eur. Phys. J. B* **2000**, *14*, 73.
(26) Roussel, P.; Labbé, Ph.; Leligny, H.; Groult, D.; Foury-Leylekian, P.; Pouget, J. P. *Phys. Rev. B* **2000**, *62*, 176.
(27) Ludecke, J.; Jobst, A.; van Smaalen, S. *Europhys. Lett.* **2000**, *49*, 357.
(28) Hess, C.; Schlenker, C.; Bonfait, G.; Ohm, T.; Paulsen, C.; Dumas, D.; Teweldemedhin, Z.; Greenblatt, M.; Marcus, J.; Almeida, M. *Solid State Commun.* **1997**, *104*, 663.
(29) Witkowski, N.; Garnier, M.; Purdie, D.; Baer, Y.; Malterre, D.; Groult, D. *Solid State Commun.* **1997**, *103*, 471.
(30) Travaglini, G.; Wachter, P.; Marcus, J.; Schlenker, C. *Solid State Commun.* **1981**, *37*, 599.
(31) McConnell, A. W.; Clayman, B. P.; Homes, C. C.; Inoue, M.; Negishi, H. *Phys. Rev. B* **1998**, *58*, 13565.
(32) Fateley, W. G.; Dollish, F. R.; McDevitt, N. T.; Bentely, F. F. *Infrared and Raman Selection Rules for Molecular and Lattice Vibrations: The Correlation Method*; Wiley-Interscience: Sussex, UK, 1972.
(33) Roussel, P.; Labbé, P.; Groult, D. *Acta Crystallogr. B* **2000**, *56*, 377.
(34) McConnell, A. W. Ph.D. Dissertation, Simon Fraser University, 1999.

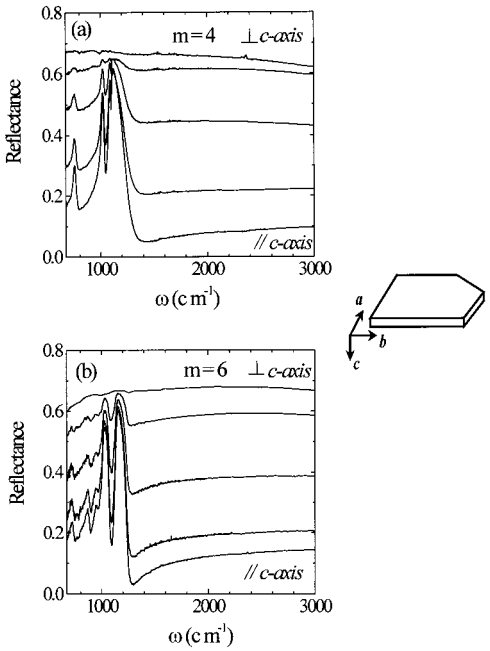

Figure 1. Polarized reflectance spectra of $m = 4$ (a) and $m = 6$ (b) MPTB single crystals. For the spectra from bottom to top, the polarization direction is 0° (∥), 30°, 50°, 70°, and 90° (⊥) to the *c*-axis.

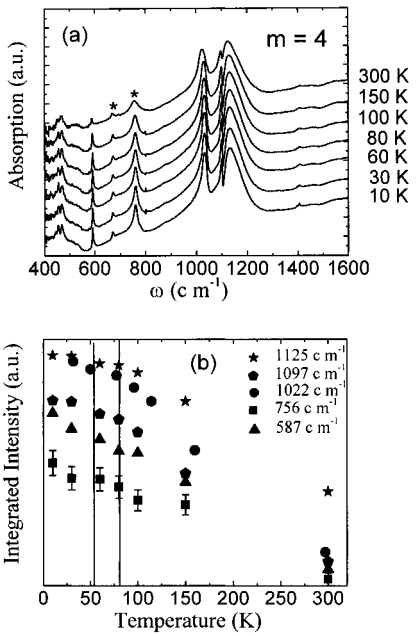

Figure 2. (a) Middle infrared absorption spectra of the $m = 4$ powder sample/KBr pellet in both normal and CDW states ($T_{c1} = 80$ K, $T_{c2} = 52$ K). The asterisk (*) indicates the mode is W−O related. The data are offset for clarity. (b) Integrated intensities of several vibrational modes as a function of temperature. Vertical lines denote CDW transition temperatures. The error bar shows 5% error.

vibrational features weaken gradually; the background reflectance increases at the same time. When the polarized light is perpendicular to the *c*-axis (i.e., parallel to the conducting *ab* plane),[35] the reflectance level is up to 0.7 and the vibrational features are screened. Thus, the electrodynamic response in the *ab* plane is metallic, whereas it is semiconducting along the *c*-axis, demonstrating the strong two-dimensional character of these monophosphate bronzes. A semiconducting interlayer response is also observed in other prototypical Q2D materials, such as cuprate superconductors (YBCO) and superconducting organic solids (κ-$(ET)_2Cu[N(CN)_2]Br$).[36,37]

If the free carrier plasma frequency is much greater than the lattice vibration frequencies,[38] a screening length can be calculated as $l_s^2 = (a_0/4)(\pi/3n)^{1/3}$. Here, a_0 is the Bohr radius and n is the free electron concentration. The estimated screening length, $l_s \approx 0.76$ Å (with $n \approx 1.6 \times 10^{22}$ and 1.25×10^{22} cm^{-3} for the $m = 4$ and $m = 6$ compounds), indicates heavily screened ionic cores. Note that the average W−O bond length is ≈2 Å,[39] so the screening length is fairly short compared to this characteristic lattice distance. The optical spectrum in the conducting plane is consistent with this expected free electron response.

The *c*-axis vibrational spectrum of the $m = 6$ compound displays several additional features compared with that of the $m = 4$ material. Further, PO_4-related vibrational modes above 1000 cm^{-1} are narrower and more well-resolved. The difference is likely due to the degree of WO_6 distortion near the PO_4 tetrahedral layer. For the $m = 4$ and 6 materials, the oxidation states of W and the W−O distances differ,[39] with the WO_6 octahedra being less distorted in the $m = 6$ compound. The PO_4 layer in the $m = 6$ compound is slightly less distorted as well, resulting in better-resolved PO_4-related vibrational features. Detailed assignments of the vibrational features along *c* will be given below.

B. Temperature Dependence. The 300 K absorption spectrum of the $m = 4$ MPTB compound is shown in Figure 2a.[40] The features in this spectrum are very similar to those in the *c*-axis reflectance spectrum (Figure 1a). That no new modes appear indicates that the unpolarized absorption spectrum presented here does not contain any additional *ab* plane vibrations. The cluster of features at 1125, 1097, and 1022 cm^{-1} are P−O−P stretching modes of the PO_4 tetrahedra;[41,42] the peaks at 668 and 756 cm^{-1} (indicated by asterisks) can be assigned as W−O−W stretching modes;[41,43,44] the small structure at 587 cm^{-1} is related to P−O bending.[41,42] That there are two W−O−W stretching modes

(35) The spectrum perpendicular to the *c*-axis is the response in the *ab* plane, but it is not along crystal axes depending on the crystal shape.

(36) Homes, C. C.; Timusk, T.; Liang, R.; Bonn, D. A.; Hardy, W. N. *Phys. Rev. Lett.* **1993**, *71*, 1645.

(37) McGuire, J. J.; Rõõm, T.; Pronin, A.; Timusk, T.; Schlueter, J. A.; Kelley, M. E.; Kini, A. M. *Phys. Rev. B.* **2001**, *64*, 094503.

(38) Homes, C. C.; McConnell, A. W.; Clayman, B. P.; Bonn, D. A.; Liang, R.; Hardy, W. N.; Inoue, M.; Negishi, H.; Fournier, P.; Greene, R. L. *Phys. Rev. Lett.* **2000**, *84*, 5391.

(39) Roussel, P.; Labbé, Ph.; Groult, D.; Domengès, B.; Leligny, H.; Grebille, D. *J. Solid State Chem.* **1996**, *122*, 281.

(40) In the transmittance spectra of the $m = 4$ and 6 materials, the vibrational modes are clearly shown. In reflectance spectra, the vibrational modes are strongly screened in the conducting *ab* plane (Figure 1), making them almost impossible to identify. Thus, the transmittance spectra have an advantage over the single-crystal reflectance spectra in this case, since we can track the changing vibrational modes from 300 K through the CDW transition temperatures. This advantage is more obvious in the $m = 6$ case. The disadvantage of the transmittance method is the loss of polarization information.

(41) Nyquist, R. A.; Kagel, R. O. *Infrared Spectra of Inorganic Compounds*; Academic Press: New York, 1971.

(42) Borel, M. M.; Leclaire, A.; Chardon, J.; Daturi, M.; Raveau, B. *Inorg. Chem.* **1991**, *29*, 3871.

(43) Salje, E. *Acta Crystallogr. A* **1975**, *31*, 360.

(44) Egdell, R. G.; Jones, G. B. *J. Solid State Chem.* **1989**, *81*, 137.

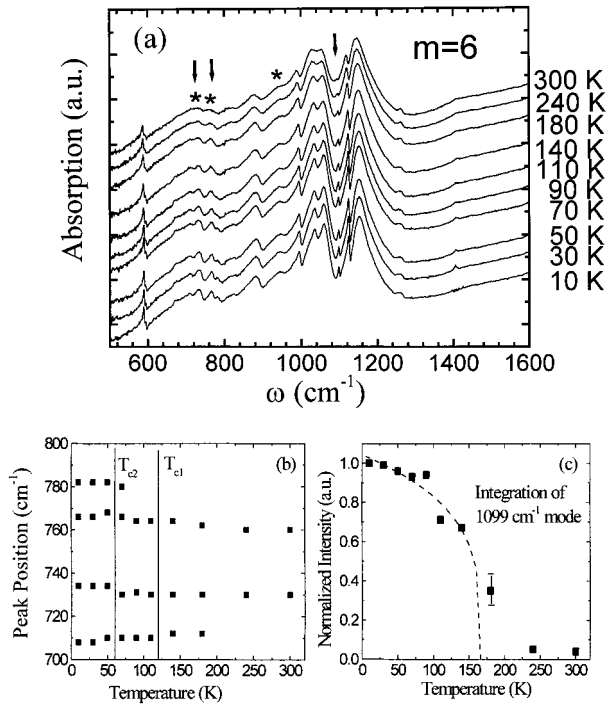

Figure 3. (a) Middle infrared absorption spectra of the $m = 6$ powder sample/KBr pellet in both normal and CDW states ($T_{c1} = 120$ K, $T_{c2} = 60$ K). Asterisk (*) indicates the mode is W−O related. Spectra are offset for clarity. (b) Peak positions of W−O stretching modes as a function of temperature. Vertical lines denote CDW transition temperatures. (c) Integrated intensity of the 1099 cm^{-1} feature as a function of temperature. The error bar shows 5% error. The dashed line is a fit of the data with $\sim(T_c - T)^{2\beta}$, where $T_c \approx 166$ K and $\beta \approx 0.13$.

at 668 and 756 cm^{-1} is likely related to the different oxidation states of W in octahedral slabs.[45]

Variable temperature measurements allow us to probe the vibrational response through the successive density wave transitions. Recall that the $m = 4$ compound has CDW transitions at $T_{c1} = 85$ K and $T_{c2} = 60$ K. Overall, the temperature dependence of the vibrational modes is weak, although most modes sharpen at low temperature. Integrated intensities of selected vibrational modes are shown as a function of temperature in Figure 2b. An interesting but small change in the W−O related mode at 756 cm^{-1} seems to correlate with the CDW effects. Changes in the 668 cm^{-1} W−O related mode with temperature are difficult to follow due to its weak intensity. In addition, the P−O bending mode at 587 cm^{-1} is also slightly sensitive to the CDW transition, as evidenced by overall softening with temperature. Higher frequency modes soften monotonically with temperature.

The absorption spectrum of the $m = 6$ compound is different from that of the $m = 4$ material, as shown in Figure 3a. The 300 K spectrum of the $m = 6$ compound has very rich vibrational structure, which not only includes the aforementioned *c*-axis modes (Figure 1b), but also suggests the appearance of a few *ab* plane modes. (For comparison, the 10 K *ab* plane reflectance spectra and calculated optical conductivity are shown in Figure 4 and discussed in the Appendix.) As in the $m = 4$ compound, the high-frequency vibrational features are assigned as P−O−P stretching modes, whereas the weak modes at 944, 761, and 730 cm^{-1} are W−O related. The broad modes at 761 and 730 cm^{-1} may be attributed to the different oxidation states of W in the $m = 6$ material. Since W atoms at the center of the conduction layers have lower oxidation states due to the more regularly shaped WO_6 octahedra,[39] such a W−O stretching mode is expected at lower frequency (730 cm^{-1}), whereas the 761 cm^{-1} mode is related to W−O stretching of W atom with a higher oxidation state and increased distortion toward the outside of the slab. The mode at 586 cm^{-1} is assigned to P−O bending, as in the spectrum of the $m = 4$ compound.

The absorption spectrum of the $m = 6$ material changes noticeably with deceasing temperature, as seen in Figure 3a.[40] Overall, the modes are sharper and more well-resolved at 10 K. Significantly, a new vibrational mode is observed at 1099 cm^{-1}, and modes at 730 and 761 cm^{-1} split into doublets upon entry into the CDW states below T_{c1} (120 K) and T_{c2} (60 K), respectively. As shown in Figure 3b, the splitting of the 730 cm^{-1} mode persists up to 180 K, well above T_{c1}, suggesting substantial fluctuation effects; the 761 cm^{-1} mode splitting also continues above T_{c2}, suggesting weaker fluctuation effects. Large fluctuation effects are also observed in other Q2D CDW oxides.[2,5] The splittings of W−O related modes indicate that strong lattice distortions are coupled with the CDW transitions in the $m = 6$ compound. Here, it is important to note that, while that the symmetry of the WO_6 octahedra is low (C_1) even at 300 K,[39] we observe the effects of increased distortion (as an apparent splitting) in the low-temperature spectra. Only the 730 cm^{-1} mode is sensitive to T_{c1}, whereas both 730 and 761 cm^{-1} modes correlate with T_{c2}. As mentioned previously, the modes at 730 and 761 cm^{-1} are likely related to WO_6 motion at the center and the edge of octahedra layer, respectively; therefore, the frequency splitting in Figure 3b suggests that the first CDW formation may be driven by an instability at the heart of the conduction layer, whereas the second transition involves the entire octahedral slab. This can be explained by strong electron−phonon interaction at the center of the octahedra layer. A similar result is anticipated for the $m = 4$ sample, in line with recent low-temperature X-ray diffraction data by Ludecke et al.[27]

The new absorption peak at 1099 cm^{-1} is likely a P−O related stretching mode, as it appears as additional low-temperature fine structure in the PO_4 mode cluster. Based on the absence of this mode in the 10 K *ab* reflectance spectra shown in the Appendix (Figure 4), this new mode is polarized along the *c*-axis. The integrated intensity of this feature as a function of temperature (Figure 3c) indicates a second-order phase transition around 120 K, where clear softening is observed, in good agreement with the value of T_{c1}. The intensity of the 1099 cm^{-1} mode at temperatures well above T_{c1} again points toward important fluctuation effects in the MPTB materials. The intensity (I) of new modes (such as phase phonons) below a transition is proportional to the square of the order parameter (Δ); i.e., $I \sim \Delta^2$.[46,47] In Figure 3c, fitting the integrated intensity as $\sim(T_c - T)^{2\beta}$ (dashed curve) yields $T_c = 166$ K and $\beta \approx 0.13$. The β value is small compared with the value in a mean field

(45) Note that W−O stretching modes of the $m = 4$ compound are at lower frequencies compared to those modes of the $m = 6$ material because of higher average oxidation states of W in the $m = 6$ material.

(0.5) [48] or a tricritical (0.25) transition,[46] indicating that these models are not applicable here.

It is interesting that the absorption spectrum of the $m = 4$ compound is dominated by *c*-axis vibrational modes at room temperature, whereas that of the $m = 6$ material exhibits a somewhat richer response. The X-ray and transport measurement have observed several differences between the $m = 4$ and 6 compounds, which might shed light on the spectral difference, although the overall physical properties of both materials are similar. First, X-ray diffuse scattering measurements of both materials reveal the existence of diffuse lines at room temperature. However, the three diffuse lines are perpendicular to the $\vec{a}$ and $\vec{a} \pm \vec{b}$ directions for $m = 4$, whereas only two diffuse lines perpendicular to $\vec{a} \pm \vec{b}$ are observed for $m = 6$.[21] Second, as reported by Hess et al., the resistivity is almost 1 order of magnitude larger in $m = 6$ than in $m = 4$ at 300 K.[49] This observation cannot be accounted for only by the carrier concentration difference, nor can it be explained by free carrier screening effects since the calculated screening lengths are nearly identical. Therefore, the different absorption spectrum and resistivity at room temperature has to be attributed to a stronger electron−phonon coupling in the $m = 6$ compound compared to the $m = 4$ material. This conclusion is consistent with a better nesting vector and higher transition temperatures for the $m = 6$ compound.[17]

The variable temperature absorption spectrum of the $m = 6$ compound suggests that a lattice distortion coincides with the CDW transitions at 120 and 60 K, indicated by the splittings of W−O modes at 730 and 761 cm^{-1} and a new mode at 1099 cm^{-1}. In contrast, a more modest coupling to the CDW transitions at 85 and 52 K is inferred from the weak temperature dependence of the $m = 4$ absorption spectrum. This is consistent with the lower dimensionality and better Fermi surface nesting of the $m = 6$ compound, as predicted by band structure calculations[17,18] and confirmed by the magnetotransport and thermopower measurements.[49−51] However, thermopower experiments also report a surprising anisotropic response in the *ab* plane for the $m = 6$ material, compared with the isotropic thermopower for the $m = 4$ material in the CDW states.[49,50] Combined with observed mode splitting and a new vibrational feature in the middle infrared absorption spectrum, the results point toward the possibility that subtle structural changes may occur along with the CDW transitions in the $m = 6$ compound. A detailed single-crystal X-ray experiment of $(PO_2)_4(WO_3)_{2m}$ ($m = 6$) at low temperature may reveal the structural change.

V. Conclusion

We have measured the middle infrared reflectance and transmittance spectra of MPTB $m = 4$ and $m = 6$ compounds. The interlayer *c*-axis reflectance spectra display strong vibrational modes with a weak electronic background, whereas the infrared spectra in the *ab* plane are highly reflective and nearly featureless, confirming the Q2D nature of both materials. Transmittance measurements, and subsequent calculated absorption spectra, allow us to follow changes in the elastic response through the density wave transitions. The vibrational modes in the absorption spectrum of the $m = 4$ compound are similar to those in the reflectance spectrum along the *c*-axis, and the temperature dependence of these modes is weak, with only the 756 cm^{-1} (related to W−O motion) feature correlating with the onset of density wave transitions. In contrast, the spectrum of the $m = 6$ material displays a richer response at 300 K. A new mode at 1099 cm^{-1} appears, and modes at 730 and 761 cm^{-1} split in the CDW states. The correlation between the oxidation states of W and the modes at 730 and 761 cm^{-1} reveals that the first CDW formation occurs largely at the center of the conduction layer, whereas the second transition seems to involve the octahedra slab as a whole. The temperature dependence of the spectrum for the $m = 6$ compound strongly suggests that a subtle crystal structure change is associated with the first CDW transition.

Acknowledgment. Work at SUNY−Binghamton and the University of Tennessee is supported by the Materials Science Division, Office of Basic Energy Sciences at the U.S. Department of Energy under Grant No. DE-FG0201-ER45885. Work at Rutgers University is supported by the National Science Foundation−Solid State Chemistry under Grant No. DMR-99-07963.

VI. Appendix

Figure 4 shows the reflectance (inset) and optical conductivity spectra of the $m = 6$ compound in the conducting *ab* plane at 10 K. The data were collected with a Bruker Equinox 55 FTIR spectrometer coupled with a Bruker IR Scope, covering the frequency range from 600 to 16 000 cm^{-1}. An Oxford Microstat He cryostat system was used for low-temperature measurements. Optical conductivity was calculated from reflectance via Kramers−Kronig transformation, with Hagen−Rubens ($R(\omega) = 1 - A\omega^{1/2}$) extrapolation toward $\omega \rightarrow 0$ and ω^{-2} for high-frequency extrapolation. Note these extrapolations do not affect the phonon frequencies in the spectral range shown in the figure.

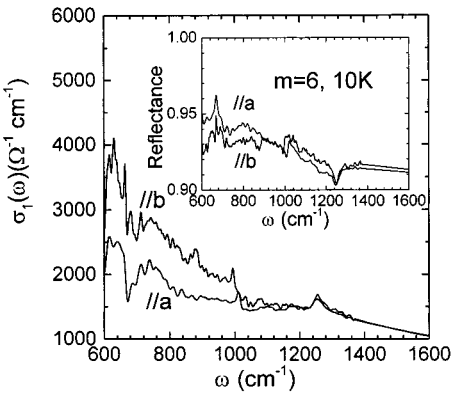

Figure 4. 10 K optical conductivity of the $m = 6$ MPTB.

CM010214V

(46) Berner, D.; Burlakov, V. M.; Scheiber, G.; Widder, K.; Geserich, H. P.; Gmeiner, J.; Schwoerer, M. *Solid State Commun.* **1996**, *97*, 863.
(47) Liu, H.-L.; Chou, L.-K.; Abboud, K. A.; Ward, B. H.; Fanucci, G. E.; Granroth, G. E.; Canadell, E.; Meisel, M. W.; Talham, D. R.; Tanner, D. B. *Chem. Mater.* **1997**, *9*, 1865.
(48) Grüner, G. *Density Waves in Solids*; Addison-Wesley: New York, 1994.
(49) Hess, C.; Schlenker, C.; Dumas, J.; Greenblatt, M.; Teweldemedhin, Z. S. *Phys. Rev. B* **1996**, *54*, 4581.
(50) Rötger, A.; Schlenker, C.; Dumas, J.; Wang, E.; Teweldemedhin, Z.; Greenblatt, M. *Synth. Met.* **1993**, *55−57*, 2670.
(51) Touze, C. L.; Nguyen, L. H.; Schlenker, C.; Steep, E.; Greenblatt, M. *Synth. Met.* **1997**, *86*, 2133.